Thermocapillary manipulation of microfluidic droplets: Theory and applications

François Gallaire, Charles N. Baroud, Jean-Pierre Delville

THERMOCAPILLARY MANIPULATION OF MICROFLUIDIC DROPLETS: THEORY AND APPLICATIONS

François Gallaire[1], Charles N. Baroud[2], Jean-Pierre Delville[3]

[1] Laboratoire JA Dieudonné, Université de Nice Sophia-Antipolis

[2] LadHyX, Ecole Polytechnique, 91128 Palaiseau Cedex

[3] CPMOH, Universté de Bordeaux I, 351 Cours de la libération, F-33405 Talence Cedex

September 12, 2007

Abstract

It was recently demonstrated by our group that a focused laser beam could be used to produce a net force on a moving microfluidic drop. The aim of the paper is to establish a scaling law for this net force by a examining the closely related but simpler situation of a very thin stationary circular drop of fixed shape submitted to a thermocapillary (Marangoni) stress. This leads us to recall the depth-averaged model for a microfluidic pancake-like undeformable drop submitted to a thermocapillary forcing. Our numerical method to solve the associated equations is then introduced and validated. In the case of a localized heating and for an 'inverse' Marangoni effect (i.e. the surface tension increases with temperature) mimicking the experimental situation of a focused laser beam impinging on a surfactant laden water-oil interface, the flow field is computed and compared to experimental observations. The viscous shear stresses (normal and tangential) and the pressure force are then computed on the interface, yielding a simple expression for the total force acting on the droplet. Further numerical investigations are conducted and enable us to propose a scaling law for the net force combining all pertinent parameters.

1. INTRODUCTION

Effective actuation of microfluidic drops may appear as simple, but when both inertial and buoyancy effects are negligible, the manipulation of water in oil drops turns out to be difficult to achieve. Furthermore, several more complicated operations are necessary if one wishes to use droplets as microreactors in microfluidic lab-on-a-chip systems. These operations include the ability to create a reaction (fusion of drops and mixing of a drop's content), test the results (sort drops), or sample their contents by dividing them asymmetrically.

We have recently demonstrated that a localized heating from a laser source on the surface of the drop may be used to produce these operations through the thermocapillary effect, by which the surface tension of an interface varies with the temperature. In our recent experiments [1], we showed that a water in oil drop, transported by the external oil flow, may be blocked if submitted to a focused laser spot. This blocking may last a few seconds, implying that the force due to the drag from the oil is balanced (at least temporarily) by a force which is generated by the laser heating. This blocking force was then combined with the geometry of the micro-channel to succeed in most of the aforementioned operations (merging, sorting and dividing).

The effect of temperature gradients on drops has been studied since the 1950's because of its applications in microgravity situations [2, 3] and has been recently revived by the applications in microfluidics [4, 5]. The generally accepted description [2, 4] is that surface tension decreases with temperature. Therefore if a drop is placed in a temperature gradient, it will experience flow along the interface from the hot to the cold side. In a low Reynolds number situation, this flow very rapidly (immediately for $Re \to 0$) produces a matching flow in the outer fluid from the hot to the cold region. Therefore by conservation of matter, the drop must "swim" towards the hot side.

This description is not compatible with our observations as deduced from figure 1 which depicts a cross-shaped microchannel in which oil

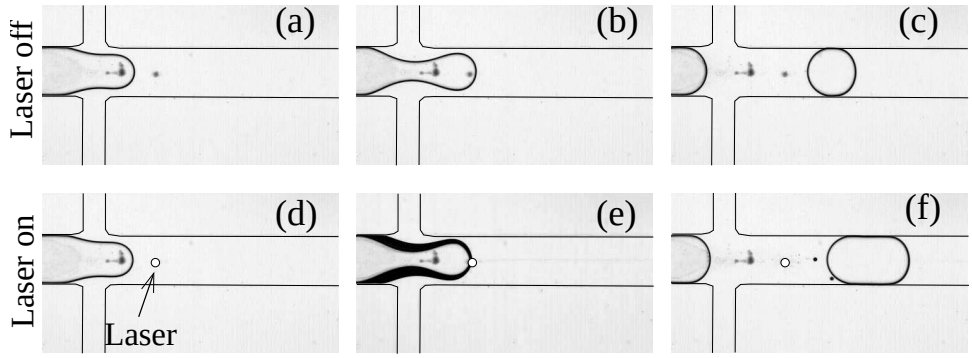

Figure 1: The water interface is temporarily blocked when it crosses the path of the focused laser in response to a force directed away from the hot spot, resulting in the production of a larger drop.

flows from the top and bottom branches and water from the left branch. Water drops in oil are produced and flow down the right hand branch in the absence of a laser. However, when the water interface crosses the laser spot, it is completely blocked, indicating that there exists a force acting from the right to the left, i.e. counteracting the viscous drag produced by the external flow. Unlike the usual Marangoni force, this force is directed from the heated region centered on the focusing point of the laser to the cold regions of the flow away from the laser thereby balancing the drag from the external oil flow and blocking the droplet.

Rather than simply ruling out a thermocapillary origin of the observed force, we have introduced tiny toner particle in the fluids in order to visualize in detail the direction of the flow in our experiments. Figure 2(a) shows that the flow is directed form the cold regions towards the hot spotalong the interface, pointing to an 'inverse' Marangoni effect. Without ignoring that, for pure liquids, the direction of Marangoni flow along the interface is directed from the hot (low surface tension) to the cold (high surface tension) regions, this opposite finding is consistent with previous studies [6, 7] which have shown an increase of surface tension with temperature in the presence of surfactants.

2. GOVERNING EQUATIONS AND NUMERICAL METHOD

Our experiments were conducted in high aspect ratio channels. The typical dimension in the transverse direction is about 500 μm, while the typical dimension in the thickness is about

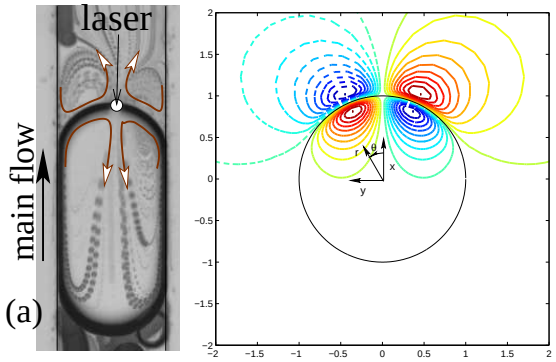

Figure 2: (a) Overlay of 100 images from a video sequence, showing the motion of seeding particles near the hot spot. Note that the motion along the interface is directed towards the hot spot. Channel width is 140 μm.(b) Streamfunction contours obtained by solving the depth-averaged model described in the text. Red contours indicate clockwise flow and blue contours indicate counter-clockwise flow. $h/R = 0.2$, $w/R = 0.5$.

20-30 μm. With typical velocities of $1mm/s$, the Reynolds number is seen to be very small. For these two reasons, we use a Hele-Shaw-like approximation, based on the depth-averaged Stokes equations as Boos and Thess [8], Bush [9] or Nadim et al. [10]. Note that, contrary to the Hele-Shaw approximation, where the depth-averaged velocity field derives from a potential and cannot fulfill the Marangoni induced tangential shear stress discontinuity at the interface, higher-order terms are kept in the equations to yield a 4^{th}-order biharmonic-type equation for the streamfunction detailed below.

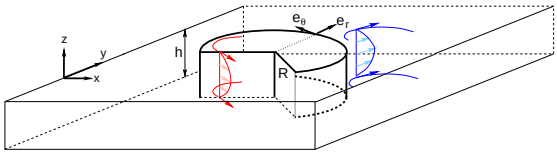

Figure 3: Schematic of the depth-averaged model.

Let us consider a circular drop of radius R in an infinite domain, as sketched in Fig 3. Assuming a parabolic profile in the small dimension (z) and introducing a streamfunction for the mean velocities in the plane of the channel, the depth averaged equations derived from the Stokes equations valid in each fluid are

$$\left(\frac{1}{r}\frac{\partial}{\partial r}r\frac{\partial}{\partial r}+\frac{1}{r^2}\frac{\partial^2}{\partial\theta^2}\right)\left(\frac{1}{r}\frac{\partial}{\partial r}r\frac{\partial}{\partial r}+\frac{1}{r^2}\frac{\partial^2}{\partial\theta^2}-\frac{12}{h^2}\right)\psi=0, \quad (1)$$

where the depth-averaged velocities may be retrieved from $u_\theta = -\partial\psi/\partial r$ and $u_r = 1/r(\partial\psi/\partial\theta)$. At the drop interface ($r = R$), two kinematic boundary conditions are imposed; zero normal velocity

$$\psi^{(1)} = \psi^{(2)} = 0, \quad (2)$$

and the continuity of the tangential velocity

$$\frac{\partial\psi^{(1)}}{\partial r} = \frac{\partial\psi^{(2)}}{\partial r}. \quad (3)$$

The normal dynamic boundary condition is not imposed since the geometry of the drop is imposed and the transverse curvature of the meniscus is assumed to counterbalance the pressure difference at the interface. Finally, the tangential dynamic boundary condition which takes into account the Marangoni stress is

$$\mu_1 r\frac{\partial}{\partial r}\left(\frac{u_\theta^1}{r}\right)-\mu_2 r\frac{\partial}{\partial r}\left(\frac{u_\theta^2}{r}\right)=-\frac{\gamma'}{r}\frac{dT}{d\theta}, \quad (4)$$

where $\mu_{1,2}$ are the dynamic viscosities and $u_\theta^{1,2}$ are the azimuthal velocities in the drop and the carrier fluid, respectively, and where $\gamma' = \partial\gamma/\partial T$ is the surface tension to temperature gradient and $T(r,\theta)$ is the imposed temperature field.

A pseudo-spectral discretization technique combining a Tchebitscheff collocation method in the radial direction with respectively $N_r^{(1)}$ and $N_r^{(2)}$ collocation points and a Fourier expansion along the azimut with N_θ modes is implemented in each fluid together with the 4 boundary conditions at the interface. The symmetry conditions at the origin in the inner fluid are taken implicitly into account as in [11] and an outer radius of $r_{max} = 8R$ is chosen to impose the far field boundary conditions in the outer fluid. The code, written in matlab, can be run on a laptop in a few minutes as long the memory requirements remain reasonable (i.e. as long as h/R is not too small, preventing the appearanceof very thin boundary layers in each fluid). The convergence of the results with increasing resolution has been checked. We use in general $N_r^1 = 40$, $N_r^2 = 40$, $N_\theta = 40$.

As a typical test-case, the Marangoni induced flow around a drop in a linear temperature gradient and with a positive surface tension to temperature gradient $\gamma' > 0$ is considered and our results are compared to the analytical solution of [8] in figure 4, displaying an excellent agreement, with errors less than 0.1% for $h/R = 0.2$.

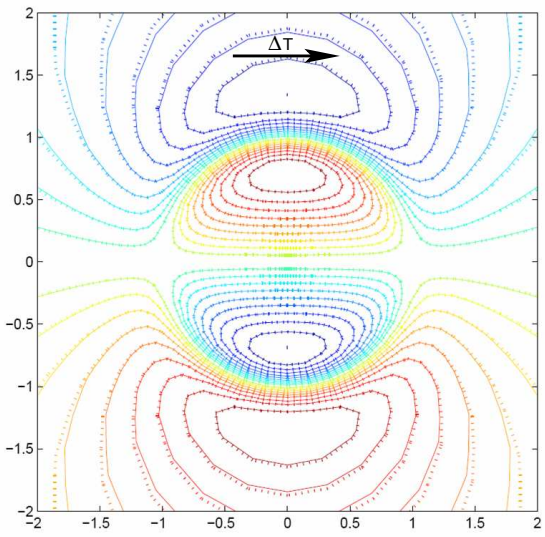

Figure 4: Superposition of the analytical solution obtained by Boos and Thess [8] (full isolines) and our numerical computation (dashed isolines) in presence of a linear temperature gradient. $h/R = 0.2$ and $\mu_2 = \mu_1$. The color convention is similar to Fig. 2b.

3. LOCALIZED HEATING

The analytical solution found by Boos and

Thess[8] is only valid for a linear temperature gradient and a numerical approach becomes compulsory when the heating is localized, so as to mimic the experiment. According to the experimental observations, the surface tension to temperature gradient γ' is taken positive and may be estimated at $\gamma' \sim 1$ mNm^{-1}K^{-1} [6, 7]. For simplicity, we approximate the steady state temperature distribution using a Gaussian form corresponding to a hot region of size w, $T(x,y) = \Delta T \exp^{-\frac{(x-R)^2+y^2}{w^2}}$, where ΔT is the maximum temperature difference between the hot spot and the far field and w corresponds to the hot spot size and is significantly larger than ω_0. The equations are subsequently made nondimensional using ΔT as temperature scale, R as length scale, $R\gamma'\Delta T$ as force scale and $\frac{\mu_1+\mu_2}{\gamma'\Delta T}$ as time scale, the remaining nondimensional groups being the aspect ratio h/R, the nondimensional spot size w/R and the viscosity ratio $\bar{\mu}_2 = \mu_2/(\mu_1+\mu_2)$. Nondimensional variables are denoted in the sequel by an overbar.

A typical flow field is shown in Fig. 2(b). As in the experimental image, and despite the difference in the drop shape and in the presence of lateral walls, four recirculation regions are clearly visible and the flow is seen to converge towards the hot region along the interface.

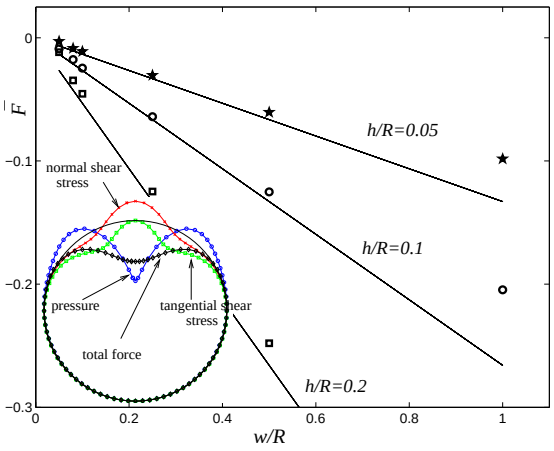

Figure 5: Nondimensional force $\bar{F}$ plotted as a function of w/R for various aspect ratios h/R (individual points) for $\bar{\mu}_2 = 3/4$. The lines correspond the asymptotic expression Eq. 14. Inset shows the distribution along the azimuthal direction of the pressure, normal and tangential shear stresses for $h/R = 0.2$, $w/R = 0.5$. Their sum yields the total force.

Three stress terms apply a net force on the drop: the pressure field as well as the viscous shear stress in the tangential and normal directions. The resulting x-component of the total force on the drop is given by the projections of these three contributions, integrated along the azimuthal direction, as shown in the inset of Fig. 5 for $h/R = 0.2$ and $w/R = 0.5$, where these three integrands and their sum are represented (once suitably normalized) as a function of the azimut by the signed distance of the corresponding curve from the unit circle. Note that the global x-component of the force is negative (the y component vanishes by symmetry) and is thereby oriented away from the laser. It may be shown in addition that the integral of the wall friction vanishes since the drop is stationary.

Let us compute the pressure field as well as the normal $\bar{\sigma}_{\bar{r}\bar{r}} = 2\bar{\mu}_2 \frac{\partial \bar{u}_{\bar{r}}}{\partial \bar{r}}$ and tangential $\left(\bar{\sigma}_{\bar{r}\theta} = \bar{\mu}_2 \left(\frac{1}{\bar{r}}\frac{\partial \bar{u}_{\bar{r}}}{\partial \theta} + \frac{\partial \bar{u}_\theta}{\partial \bar{r}} - \frac{\bar{u}_\theta}{\bar{r}}\right)\right)$ viscous shear stresses in the external flow on the interface at $\bar{r} = \bar{R} = 1$.

Since $\bar{u}_{\bar{r}}$ vanishes on the interface at $\bar{r} = 1$ independently of θ, the viscous tangential shear force reduces to

$$\bar{F}_t = -\bar{\mu}_2 \frac{h}{R} \int_0^{2\pi} \left(\frac{\partial \bar{u}_\theta}{\partial \bar{r}} - \frac{\bar{u}_\theta}{\bar{R}}\right)_{\bar{r}=1} \sin(\theta)\bar{R}d\theta$$
$$= \bar{\mu}_2 \frac{h}{R} \int_0^{2\pi} \left(-\frac{\partial \bar{u}_\theta}{\partial \bar{r}} + \bar{u}_\theta\right)_{\bar{r}=1} \sin(\theta)d\theta. \quad (5)$$

The viscous normal force is reexpressed using the continuity equation $\frac{\partial \bar{u}_{\bar{r}}}{\partial \bar{r}} = -\frac{1}{\bar{r}}\frac{\partial \bar{u}_\theta}{\partial \theta} - \frac{\bar{u}_{\bar{r}}}{\bar{r}}$ and $\frac{\partial \bar{u}_{\bar{r}}}{\partial \bar{r}}\big|_{\bar{r}=1} = -\frac{1}{\bar{r}}\frac{\partial \bar{u}_\theta}{\partial \theta}$ on the drop interface,

$$\bar{F}_n = 2\bar{\mu}_2 \frac{h}{R} \int_0^{2\pi} \left(-\frac{1}{\bar{R}}\frac{\partial \bar{u}_\theta}{\partial \theta}\right)_{\bar{r}=1} \cos(\theta)\bar{R}d\theta, \quad (6)$$

and after an integration by part

$$F_n = -2\bar{\mu}_2 \bar{h} \int_0^{2\pi} (\bar{u}_\theta)_{\bar{r}=1} \sin(\theta)d\theta. \quad (7)$$

The pressure force is given by

$$\bar{F}_p = \frac{h}{R} \int_0^{2\pi} -\bar{p}|_{\bar{r}=1} \cos(\theta)\bar{R}d\theta \quad (8)$$

An integration by parts first gives

$$\bar{F}_p = \frac{h}{R} \int_0^{2\pi} \frac{\partial \bar{p}}{\partial \theta}\bigg|_{\bar{r}=1} \sin(\theta)\bar{R}d\theta \quad (9)$$

The term $\partial\bar{p}/\partial\theta$ may be retrieved from the tangential component of the depth-averaged Stokes

equations

$$\bar{\mu}_2 \left(\frac{1}{\bar{r}} \frac{\partial}{\partial \bar{r}} \bar{r} \frac{\partial}{\partial \bar{r}} - \frac{1}{\bar{r}^2} + \frac{1}{\bar{r}^2} \frac{\partial^2}{\partial \theta^2} - \frac{12R^2}{h^2} \right) \bar{u}_\theta + \bar{\mu}_2 \frac{2}{\bar{r}^2} \frac{\partial \bar{u}_{\bar{r}}}{\partial \theta} = \frac{1}{\bar{r}} \frac{\partial \bar{p}}{\partial \theta}. \quad (10)$$

Since $\bar{u}_{\bar{r}}$ vanishes on the interface at $\bar{r} = 1$ independently of θ, the term $\frac{2}{\bar{r}^2} \frac{\partial \bar{u}_{\bar{r}}^{(2)}}{\partial \theta}$ is zero at $\bar{r} = 1$ and the pressure force becomes

$$\bar{F}_p = \bar{\mu}_2 \frac{h}{R} \int_0^{2\pi} \bar{R} \left(\left(\frac{\partial^2}{\partial \bar{r}^2} + \frac{1}{\bar{R}} \frac{\partial}{\partial \bar{r}} - \frac{1}{\bar{R}^2} + \frac{1}{\bar{R}^2} \frac{\partial^2}{\partial \theta^2} - \frac{12R^2}{h^2} \right) \bar{u}_\theta \right) \sin(\theta) \bar{R} d\theta \Big|_{\bar{r}=1}. \quad (11)$$

A double integration by parts leads

$$F_p = \bar{\mu}_2 \frac{h}{R} \int_0^{2\pi} \left(\left(\frac{\partial^2}{\partial \bar{r}^2} + \frac{\partial}{\partial \bar{r}} - 2 - \frac{12R^2}{h^2} \right) \bar{u}_\theta \right) \sin(\theta) d\theta \Big|_{\bar{r}=1}. \quad (12)$$

The final expression for the nondimensional force is obtained by adding (5), (7) and (12)

$$\bar{F} = \bar{F}_t + \bar{F}_n + \bar{F}_p = \bar{\mu}_2 \frac{h}{R} \int_0^{2\pi} \left(\frac{\partial^2}{\partial \bar{r}^2} - \frac{12R^2}{h^2} - 3 \right) \bar{u}_\theta \sin(\theta) d\theta \Big|_{\bar{r}=1}. \quad (13)$$

Results of the computations for different aspect ratios (h/R) and hot spot size (w/R) and for $\bar{\mu}_2$ are shown in Fig. 5, where it appears that the data is well fitted (see the solid lines) by an expression as simple as

$$\bar{F} \simeq -\alpha \bar{\mu}_2 \frac{h}{R} \frac{w}{R}, \quad (14)$$

with the prefactor $\alpha \simeq 3.5$. This expression may be understood by replacing the implicit (since it involves $\bar{u}_\theta$ which is deduced from the solution of the biharmonic equation (1)-(2)) expression (13) by its explicit boundary layer approximation (in the spirit of [8, 10]) in the limit where h is small compared to all characteristic in-plane length scales ($h \ll R, w$)

$$\bar{F} \simeq -2\bar{\mu}_2 \frac{h}{R} \int_0^{2\pi} \bar{T}(\bar{r} = 1, \theta) \cos(\theta) d\theta. \quad (15)$$

This expression, which requires only the knowledge of the temperature profile, may be further approximated in the limit of small w/R by

$$\bar{F} \simeq -2\sqrt{\pi} \bar{\mu}_2 \frac{h}{R} \frac{w}{R}, \quad (16)$$

in fine agreement with the fitted value of α since $2\sqrt{\pi} \simeq 3.55$. The resulting dimensional scaling is easily retrieved

$$F \simeq \frac{-2\sqrt{\pi} \Delta T \gamma' h w \mu_2}{R(\mu_1 + \mu_2)}. \quad (17)$$

With $\mu_1 = 10^{-3}$ Nm^{-2}s (water) and $\mu_2 = 3\mu_1$ (hexadecane), the calculated force is on the order of 0.1 μN, a very large force compared with optical tweezers.

4. CONCLUSION

In summary, we have experimentally and theoretically illustrated the efficiency of laser-driven localized thermocapillary stresses for microactuation of water droplets. By locally heating the oil-water interface, a net "pushing" force is produced, that may be used in various practical microfluidic applications: Controlling the timing of drop formation, controlling the size of the drop and the path that it follows when arriving at a bifurcation. The generality of the process provides a practical new way for acting on individual droplets, at any location, while working inside the robust environment of the microchannel.

Several scaling laws are favorable to this forcing technique: The dominance of surface stresses over volumetric effects at small scales and the rapidity of diffusive heat transfer while thermal inertia is reduced all lead to very rapid response time. Moreover, the force due to the laser heating decreases as $1/R$ with the drop radius R (Eq. 17) while the drag force [10] scales as R^2. Therefore the laser power necessary to counterbalance the drag force decreases with the drop size, which also favors miniaturization.

References

[1] C.N. Baroud, J.P. Delville, F. Gallaire, and R. Wunenburger. Thermocapillary valve for droplet production and sorting. *Physical Review E*, 75(4):046302, 2007.

[2] N.O. Young, J.S. Goldstein, and M.J. Block. The motion of bubbles in a vertical temperature gradient. *J. Fluid Mech.*, 6:350–356, 1959.

[3] J. Chen, Z. Dagan, and C. Maldarelli. The axisymmetric thermocapillary motion of a fluid particule in a tube. *J. Fluid Mech.*, 233:405–437, 1991.

[4] E. Lajeunesse and G.M. Homsy. Thermocapillary migration of long bubbles in polygonal tubes. ii. experiments. *Phys. Fluids*, 15:308–314, 2003.

[5] K.T. Kotz, K.A. Noble, and G.W. Faris. Optical microfluidics. *Appl. Phys. Lett.*, 85(13):2658–2660, 2004.

[6] B. Berge, O. Konovalov, J. Lajzerowicz, A. Renault, J.P. Rieu, M. Vallade, J. Als-Nielsen, G. Grübel, and J.F. Legrand. Melting of short 1-alcohol monolayers on water: Thermodynamics and x-ray scattering studies. *Phys. Rev. Lett.*, 73(12):1652–1655, 1994.

[7] E. Sloutskin, C.D. Bain, B.M. Ocko, and M. Deutsch. Surface freezing of chain molecules at the liquid-liquid and liquid-air interfaces. *Faraday Discuss.*, 129:1–14, 2005.

[8] W Boos and A Thess. Thermocapillary flow in a hele-shaw cell. *J. Fluid Mech.*, 352:305–320, 1997.

[9] J. Bush. The anomalous wake accompanying bubbles rising in a thin gap: a mechanically forced marangoni flow. *J. Fluid Mech.*, 352:283–303, 1997.

[10] A. Nadim, A. Borhan, and H. Haj-Hariri. Tangential stress and marangoni effects at a fluid-fluid interface in a hele-shaw cell. *J. Colloid and Interface Science*, 181:159–164, 1996.

[11] L. N. Trefethen. *Spectral methods in matlab*. 2000.